# An Analytical Approach to Determine the Pore Shape and Size of MCM-41 Materials from X-ray Diffraction Data

**Norihiro Muroyama,[†] Tetsu Ohsuna,[†] Ryong Ryoo,[‡] Yoshiki Kubota,[§] and Osamu Terasaki*[,†]**

*Structural Chemistry, Arrhenius Laboratory, Stockholm University, 10691 Stockholm, Sweden, National Creative Research Initiative Center for Functional Nanomaterials and Department of Chemistry, Korea Advanced Institute of Science and Technology, Taejon 305-701, Korea, and Department of Physical Science, Graduate School of Science, Osaka Prefecture University, Sakai, Osaka 590-0035, Japan*

*Received: December 12, 2005; In Final Form: April 10, 2006*

The pore shape and size of MCM-41 were studied analytically by comparing the observed powder X-ray diffraction intensities with that derived from the MCM-41 crystal structure models, with two different pore shapes, a hexagon and a circle. The powder diffraction patterns from the as-synthesized and the calcined MCM-41 were measured by a synchrotron radiation at SPring-8, Japan. The MCM-41 structure with circular and hexagonal pore shapes explains well for the as-synthesized and the calcined MCM-41 crystals, respectively. The pore size and boundary obtained by this approach agree with those obtained from an $N_2$ gas adsorption measurement combined with the Fourier synthesized density map.

## Introduction

The mesoporous silica MCM-41 is one of the M41S family synthesized by the Mobil group.[1,2] MCM-41 consists of pores arrayed with a hexagonal arrangement and silica walls between the neighboring pores. The pores of MCM-41 are filled with surfactant molecules after the synthesis (as-synthesized). Surfactant in the pores of MCM-41 can be removed by calcination so that the pores become empty (calcined). The pore size of MCM-41 is usually determined from the observation of capillary condensation in gas adsorption experiments. Since the pores must be empty for gas adsorption experiments, the pore size of the as-synthesized MCM-41 cannot be measured in this way.

Determinations of the pore size of MCM-41 by using powder X-ray diffraction (XRD) intensities have been studied since the report by the Mobil group,[2] who applied Oster and Riley's method,[3] which is an analytical calculation for XRD reflection intensities from arrayed cylindrical shells with a hexagonal arrangement. The authors concluded that "*diffraction intensities are of limited use in determining the structural nature of the pore walls*", since few strong reflection intensities could be observed. Oster and Riley's method was also used by Inagaki et al.,[4] Edler et al.,[5] and Tun and Mason.[6] Inagaki et al. described the structure of FSM-16 as a 2D (two-dimensional) hexagonal array of cylindrical shells. Since the silica wall of a cylinder overlaps with the neighbors in the model, it is difficult to apply the model to determine the structure from the observed XRD intensities. To account for the fact that relatively few reflections are typically observed, one of the characteristic features of the XRD pattern of MCM-41, Edler et al. introduced a Debye−Waller factor to the inner cylinder of the shell[5] and Tun and Mason introduced an imperfection in the hexagonal lattice.[6] Some methods for simulation of XRD intensities without analytical expressions for the homogeneous wall but with calculations using random atomic coordinates in the silica wall have also been reported. Sauer et al., for example, simulated an XRD pattern by using this method together with a parameter of fluctuation at the boundary between the pores and the walls.[7]

All of these methods assumed that the pore is circular in a cross section, although many TEM images of the MCM-41 crystals show that the pore shape of the as-synthesized crystals should rather be regarded as hexagonal. Stucky et al. discussed assuming the pore shape was a hexagon[8] and Solovyov et al. worked for this situation by using numerical calculations[9] but neither study used analytical expressions for the wall.

In the present study, analytical expressions for the MCM-41 structures with circular and hexagonal models for the pore shape are determined to retrieve the pore sizes of the as-synthesized and the calcined MCM-41 crystals by using a least-squares calculation to fit powder XRD patterns. Furthermore, the pore shapes are retrieved by Fourier reconstruction, and the pore sizes derived from a gas adsorption measurement are compared with the results of the analytical calculations.

**Structural Model.** We define a crystal model for MCM-41 as $C(\mathbf{r},z)$ by subtracting the pores $\{\epsilon \cdot B(\mathbf{r}) \cdot H(z)\} * \{L(\mathbf{r}) \cdot S(\mathbf{r})\}$ from a hexagonal shape $S(\mathbf{r})$ crystal with a homogeneous silica wall density $\rho_S$ (Figure 1)

$$C(\mathbf{r},z) = \rho_S \cdot [S(\mathbf{r}) - \{\epsilon \cdot B(\mathbf{r}) \cdot H(z)\} * \{L(\mathbf{r}) \cdot S(\mathbf{r})\}] \quad (1)$$

where $B(\mathbf{r})$ and $L(\mathbf{r})$ are functions of a rod with infinite length and a hexagonal lattice, respectively. $\mathbf{r}$ is a position vector in 2D real space. To accommodate the finite length of the rod, we introduce $H(z) = 1$ for $-Z/2 \le z \le Z/2$ and $H(z) = 0$ for otherwise, where $z$ is the coordinate perpendicular to the 2D plane and $Z$ is the length of the rod. A symbol * means an operation of the convolution. $\rho_P$ is a density of the pore inside and $\epsilon$ is defined by $\epsilon = (\rho_S - \rho_P)/\rho_S$. When the pore inside is vacuum (the same density of outside of the crystal), $\epsilon = 1$. Hereafter $\rho_S$ is taken to be 1. Two shapes of a circle and a hexagon are introduced as the pore shape (the cross-section of the channel). The crystal defined in the above has two different

* To whom correspondence should be addressed. E-mail: terasaki@struc.su.se. Fax: +46-8-163118. Tel: +46-8-162379.
[†] Stockholm University.
[‡] Korea Advanced Institute of Science and Technology.
[§] Osaka Prefecture University.

10.1021/jp0572378 CCC: $33.50 
Published on Web 05/16/2006

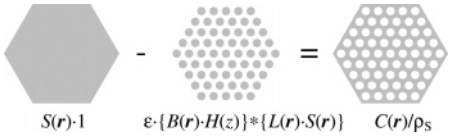


**Figure 1.** Structure model of MCM-41.

homogeneous densities in the pores and the silica wall, and any fluctuation on boundaries between the pores and the wall is not yet introduced. Since the boundary in the real MCM-41 crystals might be not flat, it is reasonable to introduce a fluctuation or gradient factor, which accommodates channel surface roughness and smoothes the average density at the boundaries between the pores and the wall. If the fluctuation is introduced by a projected function of $G(\mathbf{r})$, then eq 1 becomes

$$C(\mathbf{r},z) = G(\mathbf{r})*[S(\mathbf{r}) - \{\epsilon\cdot B(\mathbf{r})\cdot H(z)\}*\{L(\mathbf{r})\cdot S(\mathbf{r})\}] \quad (2)$$

The normalized crystal structure factor $F(\mathbf{k},k_z)$ of the crystal $C(\mathbf{r},z)$ is

$$F(\mathbf{k},k_z) = \frac{\int d\mathbf{r} \int_{-Z/2}^{Z/2} dz C(\mathbf{r},z) e^{i\mathbf{kr}} e^{ik_z z}}{\int d\mathbf{r} \int_{-Z/2}^{Z/2} dz C(\mathbf{r},z)} \quad (3)$$

$$= \frac{\mathcal{F}[C(\mathbf{r},z)]}{A} \quad (4)$$

where a wave vector is given by $\mathbf{k}$ in the 2D reciprocal space and a component perpendicular to the 2D space $k_z$ and $A$ ($= \int d\mathbf{r} \int_{-Z/2}^{Z/2} dz\ C(\mathbf{r},z)$) is a normalization factor for the forward reflection at $\mathbf{k} = (0,0)$. $\mathcal{F}$ is the Fourier transform operation. From eq 2

$$\mathcal{F}[C(\mathbf{r},z)] = \mathcal{F}[G(\mathbf{r})*\{S(\mathbf{r}) - [\epsilon\cdot B(\mathbf{r})\cdot H(z)]*[L(\mathbf{r})\cdot S(\mathbf{r})]\}] \quad (5)$$

$$= \mathcal{F}[G(\mathbf{r})]\cdot\{\mathcal{F}[S(\mathbf{r})] - \mathcal{F}[\epsilon\cdot B(\mathbf{r})]*\mathcal{F}[H(z)]\cdot\mathcal{F}[L(\mathbf{r})\cdot S(\mathbf{r})]\} \quad (6)$$

$$= FG(h,k)\cdot\{FS(h,k) - \epsilon\cdot FB(h,k)*FH(kz)\cdot FLS(h,k)\} \quad (7)$$

where $FG(h,k) = \mathcal{F}[G(\mathbf{r})]$, $FS(h,k) = \mathcal{F}[S(\mathbf{r})]$, $FB(h,k) = \mathcal{F}[B(\mathbf{r})]$, $FH(kz) = \mathcal{F}[H(z)]$, $FLS(h,k) = \mathcal{F}[L(\mathbf{r})\cdot S(\mathbf{r})]$, and $(h,k)$ are the coordinates in 2D reciprocal space, the so-called Miller indices. Although observed intensity profiles include several terms such as Lorentz, polarization, and thermal vibration factors, the intensity $I(\mathbf{k},k_z)$ is defined here by the square of the crystal structure factor

$$I(\mathbf{k},k_z) = |F(\mathbf{k},k_z)|^2 = F(\mathbf{k},k_z)\cdot F(\mathbf{k},k_z)* = \frac{\mathcal{F}[C(\mathbf{r},z)]\cdot\mathcal{F}[C(\mathbf{r},z)]*}{A^2} \quad (8)$$

When $Z$ is increased to infinity, $FH(k_z)$ becomes the $\delta$ function, $\delta(k_z)$, therefore $F(\mathbf{k},k_z)$ and $I(\mathbf{k},k_z)$ can be treated as 2D $F(\mathbf{k})$ and $I(\mathbf{k})$, respectively

$$F(\mathbf{k}) = F(\mathbf{k},k_z)$$

$$I(\mathbf{k}) = I(\mathbf{k},k_z) \quad (8')$$

In the following, we will treat the case of the infinite rod and the details of the functions introduced above are explicitly described.

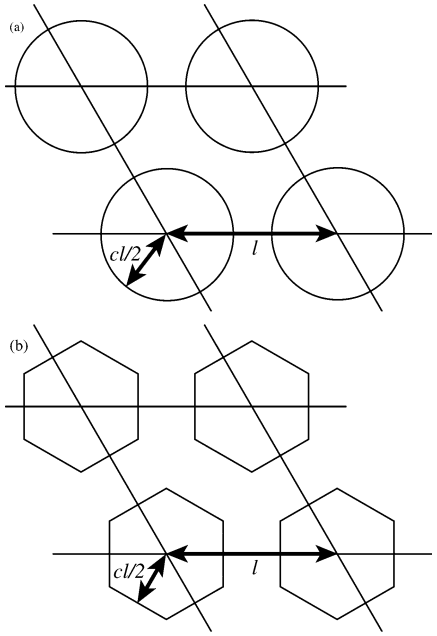


**Figure 2.** Mesopore model: (a) cylinder model and (b) hexagonal model.

**Wave Vector k.** A wave vector $\mathbf{k}$ is defined as

$$|\mathbf{k}| = \frac{4\pi \sin\theta}{\lambda}$$

where $\theta$ and $\lambda$ are a scattering angle and a wavelength, respectively. From this equation and the Bragg law ($2d_{hk} \sin\theta = \lambda$), a relationship on the hexagonal lattice between $|\mathbf{k}|$ and the unit cell length $a$ ($= 2d_{hk}((h^2 + hk + k^2)/3)^{1/2}$) is

$$|\mathbf{k}|a = 4\pi\sqrt{\frac{h^2 + hk + k^2}{3}}$$

**Pore Shape Function $B(\mathbf{r})$.** *Circular Pore.* The scattering factor of a homogeneous circular material is given by the Bessel functions.[3] Here, we introduce a parameter $c$ representing the pore size. The radius of the circle is given by $ca/2$ ($0 \le c \le 1$) (Figure 2a), and $FB(h,k)$ is

$$FB(h,k) = \frac{c\pi a J_1(c|\mathbf{k}|a/2)}{|\mathbf{k}|} = \left(\frac{a}{2}\right)^2 c\sqrt{\frac{3}{h^2 + hk + k^2}}\, J_1\left(2c\pi\sqrt{\frac{h^2 + hk + k^2}{3}}\right) \quad (9)$$

where $a$ corresponds to the distance between the nearest-neighbor circles and $J_1$ is the first-order Bessel function. When $c = 1$, a pore borders on six neighboring pores, and all pores will disappear as $c$ goes to zero.

*Hexagonal Pore.* The scattering factor of a homogeneous hexagon is

$$FB(h,k) = (a/2)^2\left[3\sqrt{3}\left\{(h-k)\cos\frac{2\pi c}{3}(h-k) - (2h+k)\cos\frac{2\pi c}{3}(2h+k) + (h+2k)\cos\frac{2\pi c}{3}(h+2k)\right\}\right] / [(h-k)(2h+k)(h+2k)\pi^2] \quad (10)$$

Here, $ca$ corresponds to the distance between the two faced edges in the hexagonal as shown in Figure 2b.

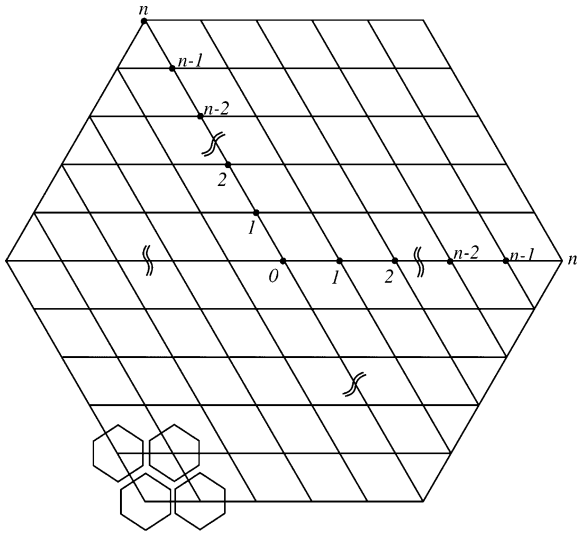


**Figure 3.** Schematic drawing to show the relationship between the lattice structure and hexagonal mesopore.

**Hexagonal Lattice Function $L(\mathbf{r})\cdot S(\mathbf{r})$.**

$$FLS(h,k) = [\sin(n+1)\pi h \sin(n+1)\pi k \sin(n+1)\pi(h+k) - \sin n\pi h \sin n\pi k \sin n\pi(h+k)]/[\sin \pi h \sin \pi k \sin \pi(h+k)] \quad (11)$$

$n$ is the number of lattice points from the center to a corner of the hexagonal crystal (Figure 3). The total number of lattice points in the crystal is given by $3n^2 + 3n + 1$. When $h$ and $k$ are integers, $FLS(h,k) = FLS = 3n^2 + 3n + 1$.

**Crystal Shape Function $S(\mathbf{r})$.** If we assume that the crystal shape is hexagonal, then $FS(h,k)$ is given by the Fourier transform of a hexagon. By taking into account that the crystal shape is rotated 30° from the hexagonal pores (see Figure 3, lower left)

$$FS(h,k) = \left(\frac{a}{2}\right)^2 \frac{\sqrt{3}\,\{h\cos Th + k\cos Tk - (h+k)\cos T(h+k)\}}{hk(h+k)\pi^2} \quad (12)$$

where $T$ depends on $n$

$$\text{Circle} \quad T = 2\pi\left(\frac{1}{\sqrt{3}} + n\right) \quad (13)$$

$$\text{Hexagon} \quad T = 2\pi\left(\frac{2}{3} + n\right) \quad (14)$$

$T$ is introduced to adjust the crystal edges toward the pore edges, but the difference between the $T$ for the circular pores and that for the hexagonal pores is not large. When $n$ is large enough, the difference is negligible and $T$ is regarded to be $2\pi n$ for both the pore shapes.

**Fluctuation or Gradient Effect $G(\mathbf{r})$.** We assume $G(\mathbf{r})$ as the Gaussian function

$$G(\mathbf{r}) = \frac{1}{2\pi\mu^2 a^2}\exp\left(\frac{-|\mathbf{r}|^2}{2\mu^2 a^2}\right) \quad (15)$$

where $\mu$ is a fluctuation parameter. The Fourier transform of $G(\mathbf{r})$ is

$$FG(h,k) = \mathrm{e}^{-(8/3)\pi^2\mu^2(h^2+hk+k^2)} \quad (16)$$

**Modulus of the Forward Reflection $A$.** The modulus of the forward reflection at $\mathbf{k} = (0,0)$ is

$$\text{Circle} \quad A = \left(\frac{a}{2}\right)^2 \{2\sqrt{3}(\sqrt{3}n+1)^2 - \epsilon c^2\pi(3n^2+3n+1)\} \quad (17)$$

Hexagon

$$A = \left(\frac{a}{2}\right)^2 2\sqrt{3}\left\{3\left(n+\frac{2}{3}\right)^2 - \epsilon c^2\pi(3n^2+3n+1)\right\} \quad (18)$$

As shown above, the four parameters are introduced to describe the crystal structure factor of the structural model for MCM-41: $n$ the number of lattice points from the center to a corner in the hexagonal crystal ($n > 0$), $c$ the ratio of the pore size to the lattice parameter $a$ ($0 \le c \le 1$), $\mu$ a fluctuation parameter ($\mu \ge 0$), and $\epsilon$ the ratio of the density of molecules within the pore to that of the silica wall ($0 < \epsilon < 1$ for the as-synthesized, $\epsilon = 1$ for the calcined).

In the present work, features of reflection intensities related to the above functions are described, followed by a comparison of the pore sizes of the as-synthesized and the calcined MCM-41 crystals as determined by using the analytical expression of the structural model together with observed XRD intensities.

## Experimental Section

MCM-41 was synthesized with the same method as previously reported.[10]

Powder XRD experiments were performed by using a synchrotron radiation at BL02B2 in SPring-8 at a wavelength of 0.108 nm. The intensity of powder diffraction is generally defined as

$$I_{\mathrm{exp}}^{\mathrm{powder}} \propto m(h,k)L(\theta)P(\theta)I(\mathbf{k})$$

where $\theta$, $m(h,k)$, $L(\theta)$, and $P(\theta)$ are a scattering angle and a multiplicity for the $h,k$ reflections, Lorentz, and polarization factors, respectively. The Debye−Waller factor is effectively included in $I(\mathbf{k})$. In this instrument, the polarization factor is 1, and the relationship between the intensity and the experimentally observed intensity, $I_{\mathrm{exp}}$, is

$$I_{\mathrm{exp}}(\mathbf{k}) \propto m(h,k)\frac{1}{\sin\theta \sin 2\theta}I(\mathbf{k})$$

The XRD patterns were analyzed by the Le Bail method in RIETAN-2000[11] to extract the reflection intensities and the unit cell parameter $a$ of the 2D hexagonal lattice. The parameters in the structural model of MCM-41 were determined by a least-squares calculation from the obtained reflection intensities. A software program for a least-squares calculation was written by N.M.

Nitrogen adsorption experiments were carried out by using ASAP2020 (Micrometrics Instrument). Pore distribution was derived by a DFT method, assuming the pore shape to be circular.

## Results and Discussions

The normalized reflection intensities calculated from eq 8′ depend on the parameters $n$, $c$, $\mu$, $\epsilon$, and the pore shape. It is important to investigate effects of varying the parameters on the relative intensities before applying the structural model to the determination of the pore size from the observed XRD reflection intensities. Since one can observe the reflection intensities in arbitrary units but cannot obtain absolute magni-

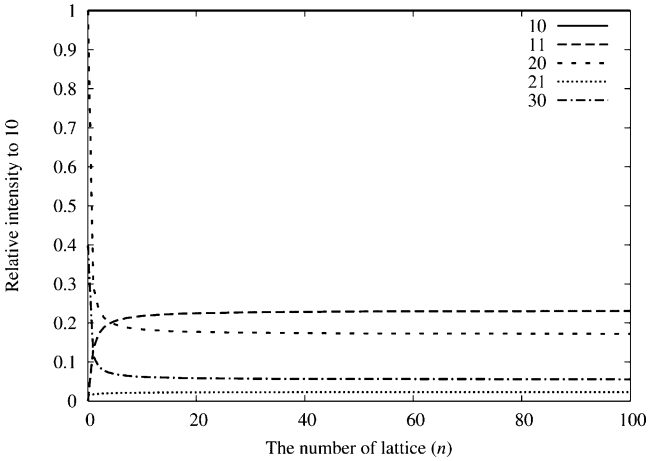


**Figure 4.** Dependence of the intensity on the parameter $n$, which gives the number of pores ($\mu = 0$, $c = 0.79$, $\epsilon = 1$).

tudes of the intensity, it is possible to discuss only relative intensity to the strongest or to the representative reflection. In the case of MCM-41, we take the 10 reflection as being representative, and hereafter, the relative normalized reflection intensity (10-relative intensity) is used in the following discussion.

***n* Dependence.** $FS(h,k)$ and $FLS(h,k)$ depend on $n$. Figure 4 shows the $n$ dependence of the 10-relative intensity with the parameters of $\epsilon = 1$, $c = 0.79$, $\mu = 0$, and the circular pore shape. All of the 10-relative intensities become independent of $n$ when $n$ becomes infinity and can be regarded as constant when $n$ is larger than ca. 40.

$$\frac{F(h,k)}{F(1,0)} = \frac{FG(h,k)\cdot\left\{\frac{FS(h,k)}{FLS} - \epsilon\cdot FB(h,k)\right\}}{FG(1,0)\cdot\left\{\frac{FS(1,0)}{FLS} - \epsilon\cdot FB(1,0)\right\}} \xrightarrow{n\to\infty} \frac{FG(h,k)\cdot FB(1,0)}{FG(h,k)\cdot FB(1,0)} \quad (19)$$

Namely, crystal size effect on the normalized intensity can be neglected when the crystal is large enough. We have confirmed from SEM images that $n$ is much larger than 160.

***c* and Pore Shape Dependence.** Figure 5 shows the $c$ dependences of the 10-relative intensities on the circular and the hexagonal pore shapes, respectively (at $n = \infty$, $\epsilon = 1$, and $\mu = 0$). Relationships (larger or smaller) between any 10-relative intensities are varying with different $c$ values. The circular pore model and the hexagonal one show similar tendencies of the relationship.

**$\epsilon$ Dependence.** When $n$ is large enough, the normalized intensity of eq 8′ is proportional to $\epsilon^2$ and the $\epsilon$ dependence of the 10-relative intensities can be disregarded in the eq 19. Figure 6 shows the $\epsilon$ dependence of the 10-relative intensities with the parameters of $c = 0.79$, $n = 50$, $\mu = 0$, and the circular pore model. When $\epsilon$ is larger than ca. 0.4, all of the 10-relative intensities can be regarded as constant.

Since the surfactant existing in the pores of the as-synthesized MCM-41 consists of hydrocarbons and the value $\epsilon$ is estimated to be 0.6 and 0.5 for the hexagonal shape and circular shape, respectively, from both the chemical analysis ($SiO_2$/surfactant) and the value $c$, the value $\epsilon$ is taken as $\epsilon = 0.5$.

***μ* Dependence.** Only $FG(h,k)$ depends on $\mu$. $G(\mathbf{r})$ is introduced to represent the fluctuation on boundaries between the pores and the walls. When $G(\mathbf{r})$ is ignored ($\mu = 0$), eq 8′ consists of trigonometric functions and a Bessel function, and the reflection intensities decay oscillatorily, but the 10-relative intensities remain higher at higher scattering angles when compared with the observed XRD pattern. $G(\mathbf{r})$ makes the 10-relative intensities reduce rapidly with increasing scattering angles.

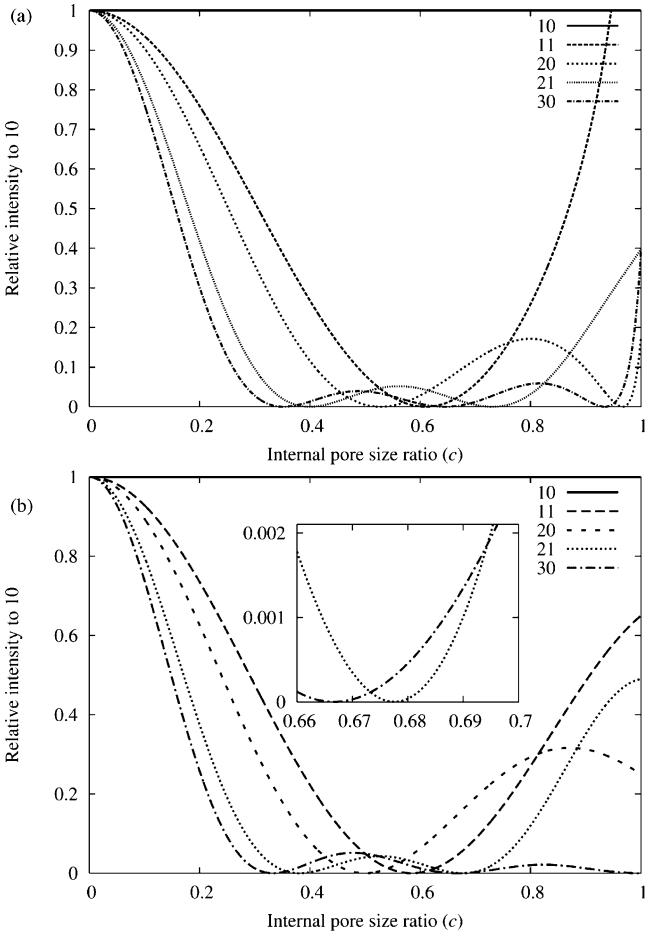


**Figure 5.** Dependence of the intensity on the pore size parameter, $c$ ($n = \infty$, $\mu = 0$, $\epsilon = 1$): (a) circular shape and (b) hexagonal shape.

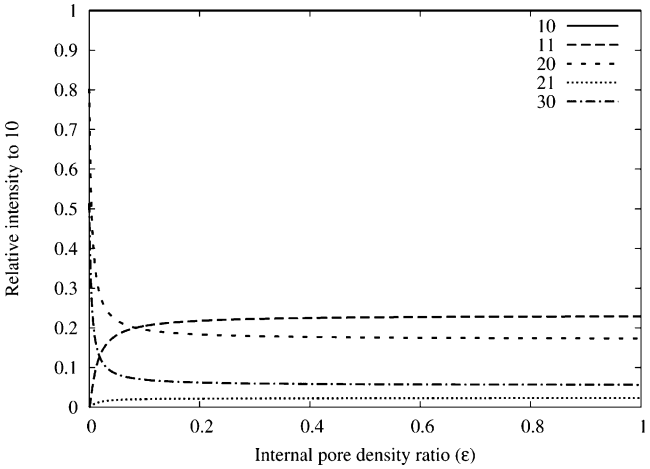


**Figure 6.** Dependence of the intensity on the density ratio, $\epsilon$ ($n = 50$, $\mu = 0$, $c = 0.79$).

The synchrotron XRD patterns of the as-synthesized and the calcined MCM-41 are shown in Figure 7. Extracted 10-relative intensities from the XRD patterns are shown in Table 1. Since the synchrotron X-ray radiation has high coherency and high-quality specimens were used, we were able to obtain five reflection intensities from both the as-synthesized and the calcined specimens.

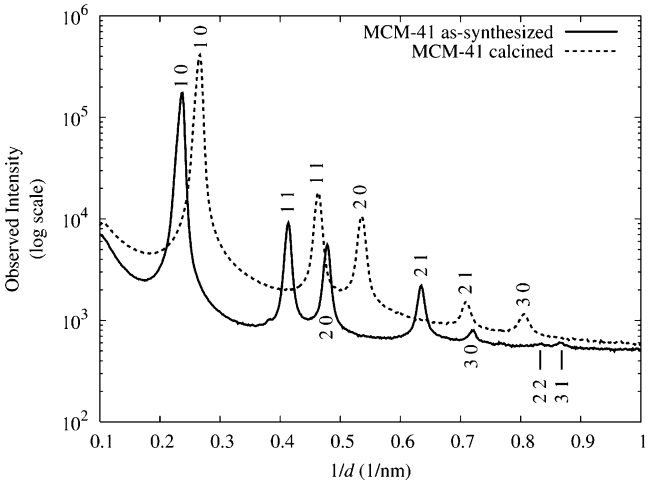


**Figure 7.** Observed powder XRD pattern for as-synthesized and calcined MCM-41 samples.

**TABLE 1: 10-Relative Intensities Retrieved from Observed XRD Patterns**[a]

| reflection | 10 | 11 | 20 | 21 | 30 |
|---|---|---|---|---|---|
| as-synthesized | 1 | 0.17(2) | 0.14(2) | 0.048(14) | 0.018(13) |
| calcined | 1 | 0.156(15) | 0.141(16) | 0.009(4) | 0.017(8) |

[a] The values in parentheses show standard deviations.

**TABLE 2: Results of the Least-square Fitting Calculation**

(a) Parameters to Give the Best Fit for the Observed Intensities

| | | *a* (nm) | c | $\mu$ | $R_I$ |
|---|---|---|---|---|---|
| as-synthesized | circle | 4.855(1) | 0.787(15) | 0.043(8) | 15.4% |
| | hexagon | | 0.82(3) | 0.070(9) | 10.6% |
| calcined | circle | 4.3075(9) | 0.770(9) | 0.037(8) | 5.9% |
| | hexagon | | 0.791(17) | 0.067(2) | 10.5% |

(b) Simulated 10-Relative Intensities and Phases by Using the Parameters Given in (a)

| reflection | 10 | 11 | 20 | 21 | 30 |
|---|---|---|---|---|---|
| as-synthesized | 1 | 0.18(2) | 0.14(2) | 0.033(8) | 0.0025(13) |
| calcined | 1 | 0.156(12) | 0.135(12) | 0.006(2) | 0.027(6) |
| phase | $\pi$ | 0 | 0 | $\pi$ | $\pi$ |

The parameters of $c$ and $\mu$ derived as fitting parameters of the least-squares calculation by using eq 8′ and the observed reflection intensities are shown in Table 2. In the calculation, it is assumed that $n = 50$ and $\epsilon = 0.5$ for the as-synthesized and $\epsilon = 1$ for the calcined sample. The residual $R_I$ ($R_I$ is defined as $\sum (I_{cal} - I_{obs})^2/\sum I_{obs}^2$) of the calculation in Table 2 suggests that the pore shape of the as-synthesized sample may be regarded as a hexagon and that of the calcined sample as a circle. The value of the parameter $\mu$ represents the magnitude of the fluctuation on the boundary between the pores and the wall, in the other words, a roughness on the wall surface. The $\mu$ value of 0.07 of the as-synthesized sample with the hexagonal pore shape corresponds to 0.2 nm of the surface roughness on the wall, which is defined as the distance from the boundary between the pores and the wall to a point of a half value of the boundary density between the pores and the wall, and $\mu = 0.037$ of the calcined sample with the circular pore shape corresponds to 0.1 nm. Figure 8 shows the density distribution maps calculated with the structural model parameters ($c$ and $\mu$ are the fitting results) for the as-synthesized (hexagonal pore) and the calcined (circular pore), respectively. One can see in Figure 8a that the map shows rounded hexagonal density distribution even though the pore shape in the structural model is hexagonal,

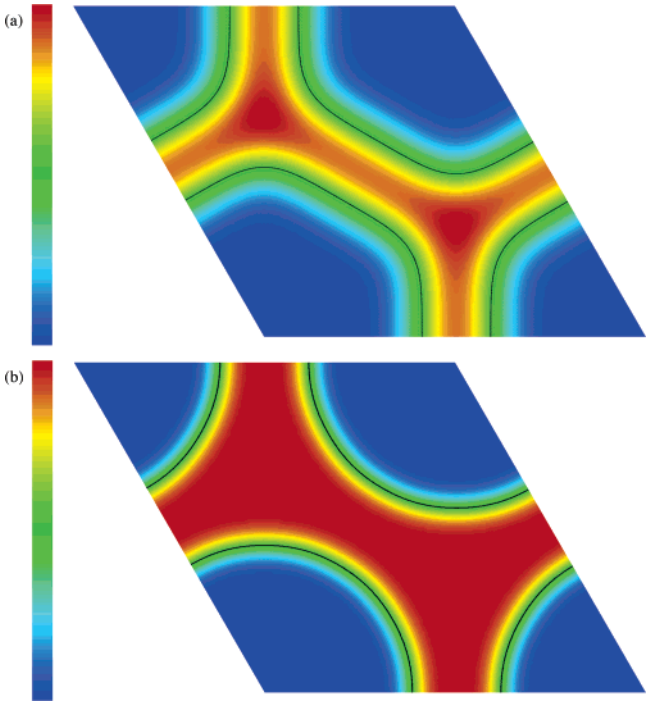


**Figure 8.** Structure obtained from the refined parameters (Table 2a): (a) as-synthesized structure and (b) calcined structure.

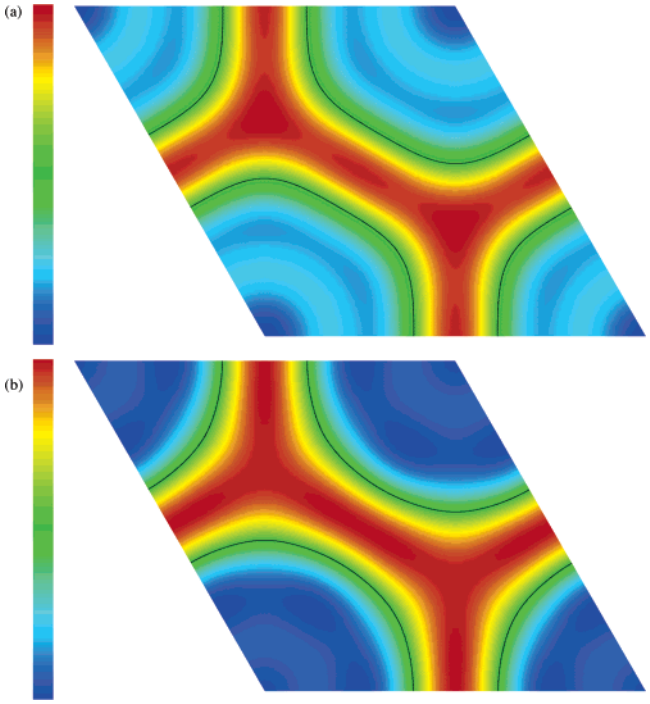


**Figure 9.** Reconstruction map obtained from the observed reflections with calculated phases (Table 1): (a) as-synthesized and (b) calcined.

as a result of the fluctuation. To obtain the pore shape (the boundary between the pore and the wall) in the rounded hexagonal distribution, a threshold density ratio, which is determined as the value at the point differing by $ca/2$ from the pore center along the hexagonal lattice axis, was observed as 0.55. The black curves in Figure 8a show contour lines corresponding to the threshold density ratio of 0.55. In the case of the calcined sample, the threshold density was determined as 0.52 by the same way as the as-synthesized sample. The boundaries in the density distribution of the calcined sample (shown by the black lines in Figure 8b) show circular shape.

**TABLE 3: Pore Diameter, Wall Thickness, Pore Area, and Wall Area**

| | pore diameter $ca$ (nm) | wall thickness $a - ca$ (nm) | pore area (nm$^2$) | wall area (nm$^2$)[c] |
|---|---|---|---|---|
| as-synthesized (hexagon) | 3.98(15) | 0.87(13) | 8.9(8)[a] | 4.8(1.1) |
| calcined (circle) | 3.32(4) | 0.99(4) | 5.12(12)[b] | 4.4(0.2) |
| difference[d] | −0.66(15) | +0.12(14) | −3.8(8) | −0.4(1.1) |

[a] The pore area of the as-synthesized is obtained by counting in the area of the density ratio below 0.52. [b] The pore area of the calcined is calculated as $\pi(ca/2)^2$. [c] Both wall areas of the as-synthesized and the calcined are obtained by subtracting pore area from unit cell area $(3)^{1/2}a^2/2$. [d] Differences are obtained by subtracting the values of the calcined from that of the as-synthesized.

**TABLE 4: Calculated Phases for the Fourier Reconstruction[a]**

| | | | | | |
|---|---|---|---|---|---|
| reflection | 10 | 11 | 20 | 21 | 30 |
| phase | $\pi$ | 0 | 0 | $\pi$ | $\pi$ |

[a] Structure factors were calculated by using eq 4 with parameters of $c = 0.789$ (3.4/4.3075), $\mu = 0$, $n = 50$, and circular pore shape.

The pore sizes, the wall thicknesses, and the differences between the as-synthesized and the calcined samples calculated from the fitting results are shown in Table 3. It is clear from Table 3 that the silica wall thickness does not change from the as-synthesized to the calcined crystals so much. The result suggests that the main origin of the lattice constant reduction in MCM-41 by calcination is regarded to be not the wall shrinkage but reduction in the pore size.

To confirm the usefulness of the analytical calculation based on the structural model, the density distributions of the as-synthesized and the calcined samples as shown in Figure 9 were retrieved by a Fourier reconstruction method using the observed XRD intensities together with the calculated phases (as shown in Table 4, which are exactly the same as the phases in Table 2a) of structure factors which were calculated from eq 4 with a pore size from the adsorption measurement as a diameter of 3.4 nm. The contour lines in Figure 9b showing the boundaries between the pores and the silica wall are determined by the adsorption result, and this threshold contour line density is 0.52. The pore size and the threshold density of the Fourier reconstruction show good agreement with that of the calcined sample derived by the least-squares calculation result. It is impossible to obtain a pore size of the as-synthesized sample by adsorption measurements, therefore the threshold density ratio for drawing boundaries in the density distribution of the as-synthesized sample was tentatively chosen in the same value as the calcined sample. The black contour lines in Figure 9a show round hexagons similar to those in Figure 8a. These agreements between the least-squares calculation results and that of the Fourier reconstruction strongly suggest that the structural model and the analytical expression of the reflection intensities are suitable for a determination of the pore size in the real MCM-41 crystals by the XRD experiments.

## Conclusion

The synchrotron powder XRD patterns of both the as-synthesized and the calcined MCM-41 crystals were analyzed analytically by (i) taking the circular and hexagonal models for the pore shape and (ii) introducing the fluctuation of the boundary between the silica wall and surfactant templates. The analysis suggested that the as-synthesized crystal has a channel with a rounded hexagon and the calcined has that with a circle. The pore size and the boundary obtained by this approach agreed with those obtained from the $N_2$ adsorption measurement combined with the Fourier synthesized density map. This approach also makes it possible to discuss the shape and size of the pores from the as-synthesized crystals, which cannot be done by $N_2$ adsorption measurement.

**Acknowledgment.** The authors thank Prof. M. Takata, Drs. K. Kato and K. Ohsaka, and JASRI, for scientific encouragement and technical supports. Figures 8 and 9 were drawn with VENUS developed by Dilanian and Izumi. This work has been partially supported by the Swedish Science Council, VR, and Japan Science and Technology Agency, JST. The synchrotron radiation experiments were performed at SPring-8 BL02B2 under JASRI/SPring-8 Nanotechnology Support Project program of the Ministry of Education, Culture, Sports, Science and Technology of Japan. Y.K. and R.R. acknowledge supports from the Grant-in-Aid for Scientific Research from the Ministry of Education Culture, Science, Sports and Technology of Japan and Creative Research Institute Program of the Korean Ministry of Science and Technology, respectively.

## References and Notes

(1) Kresge, C. T.; Leonowicz, M. E.; Roth, W. J.; Vartuli, J. C.; Beck, J. S. *Nature* **1992**, *359*, 710.

(2) Beck, J. S.; Vartuli, J. C.; Roth, W. J.; Leonowicz, M. E.; Kresge, C. T.; Schmitt, K. D.; Chu, C. T. W.; Olson, D. H.; Sheppard, E. W.; McCullen, S. B.; Higgins, J. B.; Schlenker, J. L. *J. Am. Chem. Soc.* **1992**, *114*, 10834.

(3) Oster, G.; Riley, D. P. *Acta Crystallogr.* **1952**, *5*, 272.

(4) Inagaki, S.; Sakamoto, Y.; Fukushima, Y.; Terasaki, O. *Chem. Mater.* **1996**, *8*, 2089.

(5) Edler, K. J.; Reynolds, P. A.; White, J. W.; Cookson, D. *J. Chem. Soc., Faraday. Trans.* **1997**, *93*, 199.

(6) Tun, Z.; Mason, P. C. *Acta Crystallogr. Sect. A: Found. Crystallogr.* **2000**, *56*, 536.

(7) Sauer, J.; Marlow, F.; Schüth, F. *Phys. Chem. Chem. Phys.* **2001**, *3*, 5579.

(8) Stucky, G. D.; Monnier, A.; Schüth, F.; Huo, Q.; Margolese, D. I.; Kumar, D.; Krishnamurty, M.; Petroff, P. M.; Firouzi, A.; Janicke, M.; Chmelka, B. F. *Mol. Cryst. Liq. Cryst.* **1994**, *240*, 187.

(9) Solovyov, L. A.; Kirik S. D.; Shmakov, A. N.; Romannikov, V. N. *Microporous Mesoporous Mater.* **2001**, *44*−*45*, 17.

(10) Kruk, M.; Jaroniec, M.; Sakamoto, Y.; Terasaki, O.; Ryoo, R.; Ko, C. H. *J. Phys. Chem. B.* **2000**, *104*, 292.

(11) Izumi, F.; Ikeda, T. *Mater. Sci. Forum* **2000**, *321*−*324*, 198.